Cell

Curved EFC/F-BAR-Domain Dimers Are Joined End to End into a Filament for Membrane Invagination in Endocytosis

Atsushi Shimada,[1,10] Hideaki Niwa,[1,10] Kazuya Tsujita,[2,10,11] Shiro Suetsugu,[2,3,4,10] Koji Nitta,[5] Kyoko Hanawa-Suetsugu,[6] Ryogo Akasaka,[6] Yuri Nishino,[1] Mitsutoshi Toyama,[6] Lirong Chen,[7] Zhi-Jie Liu,[7,12] Bi-Cheng Wang,[7] Masaki Yamamoto,[1] Takaho Terada,[6] Atsuo Miyazawa,[1] Akiko Tanaka,[6] Sumio Sugano,[8] Mikako Shirouzu,[6] Kuniaki Nagayama,[5] Tadaomi Takenawa,[2,11,*] and Shigeyuki Yokoyama[1,6,9,*]

[1] RIKEN SPring-8 Center, Harima Institute, 1-1-1 Kouto, Sayo, Hyogo 679-5148, Japan
[2] Department of Biochemistry, Institute of Medical Science, The University of Tokyo, Shirokanedai, Minato-ku, Tokyo 108-8639, Japan
[3] PRESTO, JST, 4-1-8, Honcho, Kawaguchi City, Saitama 332-0012, Japan
[4] Institute of Molecular and Cellular Biosciences, The University of Tokyo, Yayoi, Tokyo 113-0032, Japan
[5] Okazaki Institute For Integrative Bioscience, National Institutes of Natural Sciences, Myodaiji-cho, Okazaki 444-8787, Japan
[6] RIKEN Genomic Sciences Center, 1-7-22 Suehiro-cho, Tsurumi, Yokohama 230-0045, Japan
[7] Department of Biochemistry and Molecular Biology, University of Georgia, Athens, GA 30603, USA
[8] Department of Medical Genome Sciences, Graduate School of Frontier Sciences
[9] Department of Biophysics and Biochemistry, Graduate School of Science
The University of Tokyo, Tokyo 113-0033, Japan
[10] These authors contributed equally to this work.
[11] Present address: Kobe University Graduate School of Medicine, 7-5-1, Kusunokicho, Chuo- ku, Kobe 650-0017 Hyogo, Japan.
[12] Present address: National Laboratory of Biomacromolecules, Institute of Biophysics, Chinese Academy of Sciences, 15 Datun Road, Chaoyang District, Beijing 100101, China.
*Correspondence: takenawa@med.kobe-u.ac.jp (T.T.), yokoyama@biochem.s.u-tokyo.ac.jp (S.Y.)
DOI 10.1016/j.cell.2007.03.040

SUMMARY

Pombe Cdc15 homology (PCH) proteins play an important role in a variety of actin-based processes, including clathrin-mediated endocytosis (CME). The defining feature of the PCH proteins is an evolutionarily conserved EFC/F-BAR domain for membrane association and tubulation. In the present study, we solved the crystal structures of the EFC domains of human FBP17 and CIP4. The structures revealed a gently curved helical-bundle dimer of ~220 Å in length, which forms filaments through end-to-end interactions in the crystals. The curved EFC dimer fits a tubular membrane with an ~600 Å diameter. We subsequently proposed a model in which the curved EFC filament drives tubulation. In fact, striation of tubular membranes was observed by phase-contrast cryo-transmission electron microscopy, and mutations that impaired filament formation also impaired membrane tubulation and cell membrane invagination. Furthermore, FBP17 is recruited to clathrin-coated pits in the late stage of CME, indicating its physiological role.

INTRODUCTION

Cell membranes change their shapes upon various activities, such as cytokinesis, cell motility, and endocytosis (Farsad and De Camilli, 2003; McMahon and Gallop, 2005; Zimmerberg and Kozlov, 2006). In these processes, a number of membrane-associated proteins are involved in the generation of membrane curvature. These include dynamins, amphiphysins, endophilins, and epsins, which all play a role in clathrin-mediated endocytosis (CME) and deform liposomes into tubules in vitro through different mechanisms. Dynamins form ring- or spiral-like filaments, which constrain the lipid bilayer into a tubular shape of about 200 Å in diameter (Takei et al., 1995; Hinshaw and Schmid, 1995; Schweitzer and Hinshaw, 1998; Chen et al., 2004; Roux et al., 2006). Amphiphysins and endophilins possess the Bin/amphiphysin/Rvs (BAR) domain, which itself can deform the lipid bilayer into a tubule of ~200 Å or larger in diameter (Takei et al., 1999). This tubulation activity is mainly attributed to the intrinsic banana-like shape of the BAR-domain homodimer, which binds to the membrane with its concave surface (Peter et al., 2004). Epsins insert an amphipathic α helix into one leaflet of the lipid bilayer, which results in an area difference between the inner and outer membrane leaflets, leading to membrane tubulation (Ford et al., 2002). Endophilin BAR domains use a similar insertion

mechanism to cause membrane curvature (Masuda et al., 2006; Gallop et al., 2006).

CME plays an important role in receptor internalization, synaptic vesicle recycling, and somatic nutrient uptake (Perrais and Merrifield, 2005). The formation of clathrin-coated vesicles (CCVs) involves three steps (Merrifield et al., 2005; Kaksonen et al., 2005; Perrais and Merrifield, 2005). First, the clathrin coat assembles on the flat membrane with other proteins, such as AP-2, and captures the cargo to form a hemispherical clathrin-coated pit (CCP). Second, the CCP slowly invaginates, and the actin polymerizes. Third, scission proteins are recruited to the neck of the invaginated CCP for the separation of the newly formed CCV from the plasma membrane. Epsins participate in the initial clathrin assembly and CCP formation steps (Ford et al., 2002), while dynamins play a role in the scission step (Praefcke and McMahon, 2004). The BAR-domain proteins are involved in multiple steps of endocytosis, among which their involvement in the scission step may be the most common function in CME (McMahon and Gallop, 2005; Kaksonen et al., 2005; Ren et al., 2006).

Pombe Cdc15 homology (PCH) proteins are involved in a wide variety of actin-based processes, such as cytokinesis, filopodia formation, CME, and clathrin-independent endocytosis (Lippincott and Li, 2000; Kessels and Qualmann, 2004; Ho et al., 2004; Itoh and De Camilli, 2006; Dawson et al., 2006). The PCH proteins are characterized by the presence of an evolutionarily conserved FER-CIP4 homology (FCH) domain, and they induce tubular membrane invagination in vivo and deform liposomes into tubules in vitro (Aspenström, 1997; Lippincott and Li, 2000; Itoh and De Camilli, 2006; Dawson et al., 2006). The membrane binding and tubulation activities of the PCH proteins were attributed to a domain of ~300 amino acid residues encompassing the FCH domain and an adjacent coiled-coil region, which has been redefined as the extended FCH (EFC) or FCH and BAR (F-BAR) domain (Itoh et al., 2005; Tsujita et al., 2006). The EFC domain shares weak sequence homology with the BAR domain, and like the self-association of the BAR domain in dimer formation, it also self-associates (Kessels and Qualmann, 2004; Itoh and De Camilli, 2006; Dawson et al., 2006). A clear difference exists between the EFC- and BAR-induced tubular membranes: the diameters of the EFC-induced tubular membranes are several times larger than those of the tubular membranes induced by the BAR domain, as revealed by in vitro liposome tubulation experiments (Itoh et al., 2005; Tsujita et al., 2006). The tubular membrane invagination induced by the PCH proteins may be the outcome of imbalanced endocytic vesicle formation caused by enhanced invagination and/or a deficiency of dynamin- and actin polymerization-dependent scission (Itoh et al., 2005; Tsujita et al., 2006).

Most of the PCH proteins contain Src homology 3 (SH3) domains at the carboxyl terminus, and these domains bind to various target molecules, including dynamins and neural Wiskott-Aldrich syndrome protein (N-WASP) (Lippincott and Li, 2000; Kessels and Qualmann, 2004; Itoh and De Camilli, 2006; Tsujita et al., 2006; Dawson et al., 2006; Takenawa and Suetsugu, 2007). N-WASP plays a primary role in actin nucleation in various cytoskeletal processes (Miki and Takenawa, 2003). The actin dynamics are crucial for the scission step of CME (Merrifield et al., 2005; Kaksonen et al., 2006).

Formin-binding protein 17 (FBP17), Cdc42-interacting protein 4 (CIP4), and transducer of Cdc42-dependent actin assembly (Toca-1) share high sequence homology among each other and constitute a clearly defined subfamily in the PCH protein family (Ho et al., 2004), and thus they are designated hereafter as FBP17/CIP4-related PCH (FCRP) proteins. The FCRP proteins participate in filopodia formation and in clathrin-dependent and -independent endocytosis (Ho et al., 2004; Itoh and De Camilli, 2006; Dawson et al., 2006).

To better understand the mechanisms of membrane tubulation by the EFC domain, we solved the crystal structures of the EFC-domain dimers of human FBP17 and CIP4 at 2.6 and 2.3 Å resolution, respectively. The structures exhibit a gently curved six-helix bundle, which binds and tubulates the lipid membrane with its concave surface. Both proteins form a filament in the crystals, and the filament formation is required for their tubulation activities. On this structural basis, we proposed a mechanistic model in which a ring- or spiral-like EFC filament winds around the tubular membrane. In striking agreement with this model, phase-contrast cryo-transmission electron microscopy (cryo-TEM) revealed striation of the tubular membranes. FBP17 was recruited to the CCPs late in CME, suggesting that it plays a role in the invagination and/or scission steps in CME.

RESULTS

Overall Structures of the EFC Domains of Human FBP17 and CIP4

Initial expression trials in a cell-free translation system, using 26 constructs of human CIP4 with different N- and C-terminal boundaries, yielded several soluble fragments. Among them, one fragment, EFCΔN_{CIP4} (residues 10–303), was expressed at the highest level and yielded crystals suitable for structure determination. After the structure determination of EFCΔN_{CIP4}, the crystals of a human FBP17 fragment, EFC_{FBP17} (residues 1–300), were obtained and the crystal structure was determined by the molecular replacement method, using the structure of EFCΔN_{CIP4} as a search model. The models were built for residues 10–56 and 64–288 for EFCΔN_{CIP4} and residues 1–56 and 64–288 for EFC_{FBP17}. The rest of the residues could not be modeled due to poor/disordered electron densities. The two crystal structures are similar to each other, in agreement with the high amino acid sequence identity for the corresponding regions between FBP17 and CIP4 (54%, Figures 1A, 1D, and S1B). Superimposition of the EFC-domain structures gave an rmsd of 2.15 Å between the corresponding Cα atoms over 272

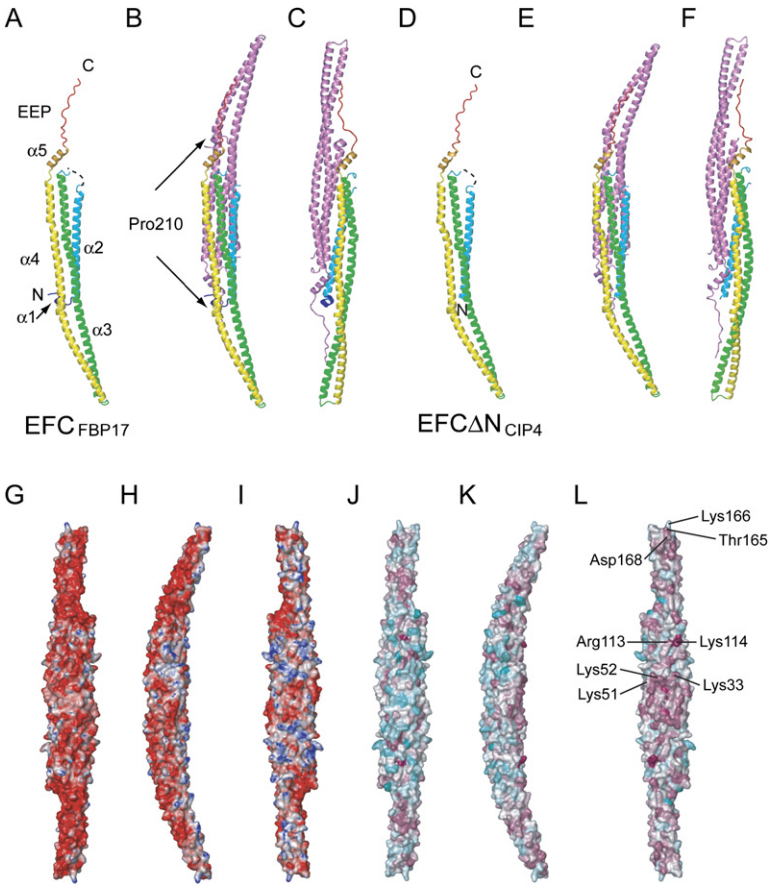

Figure 1. Three-Dimensional Structures of EFC_{FBP17} and $EFC\Delta N_{CIP4}$

(A) Ribbon diagram of the structure of EFC_{FBP17}. N and C indicate the amino and carboxyl termini of the molecule. The secondary structure elements are colored as in Figure S1B. Broken lines indicate regions that could not be modeled.

(B) Side view of the EFC_{FBP17} dimer. One molecule is depicted as in (A), while the other molecule is colored magenta.

(C) Top view of the EFC_{FBP17} dimer. The dimer is rotated by 90° relative to (B).

(D) Ribbon diagram of the structure of $EFC\Delta N_{CIP4}$. N and C indicate the amino and carboxyl termini of the molecule. The secondary structures are colored as in (A). Broken lines indicate regions that could not be modeled.

(E) Side view of the $EFC\Delta N_{CIP4}$ dimer. The molecules are depicted as in (B).

(F) Top view of the $EFC\Delta N_{CIP4}$ dimer. The dimer is rotated by 90° relative to (E).

(G–I) Electrostatic potential surfaces of the EFC_{FBP17} dimer, indicated with blue as positive and red as negative. (G) Top view (convex side); (H) side view; (I) bottom view (concave side).

(J–L) Conserved surface residues of the EFC_{FBP17} dimer. The surface is colored according to the rate of sequence conservation among the 70 PCH protein sequences (Pupko et al., 2002) in a gradient from cyan (most variable residues) to white to magenta (most highly conserved residues). (J) Top view (convex side); (K) side view; (L) bottom view (concave side). Residues mutated in the present and previous studies are indicated.

residues (Figures S2A and S2B). The structure of the EFC domain is composed of a short N-terminal helix, three long α helices, and a short C-terminal helix followed by an extended peptide of 17 amino acids (Figure 1A). $EFC\Delta N_{CIP4}$ lacks helix α1, as the N-terminal region of nine residues is deleted (Figure 1D). The classical FCH domain, defined as the N-terminal ca. 60-residue sequence, corresponds to helix α2 in our structures (Figures 1A, 1D, and S1B). From the present structures, it is now evident that all five helices, including helix α2, constitute a structurally integrated domain (Figures 1A and 1D). The C-terminal 17-residue extended peptide is also part of the structural domain, as it is involved in homodimerization (see below). We hereafter designate this peptide (residues 272–288) as the EFC extended peptide (EEP). Together, residues 1 and 288 of FBP17 define the structural domain boundaries, which agree well with those identified as the functional domain for membrane interaction (Itoh et al., 2005; Tsujita et al., 2006).

The EFC-Domain Dimer

Helices α2, α3, and α4 form an intimately packed, six-helix bundle with a neighboring symmetry-related molecule, resulting in a gently curved dimer (Figures 1B, 1C, 1E, 1F, S2A, and S2B). The EFC-domain dimers bury large areas of the dimer interfaces (4765 and 4020 $Å^2$ per molecule for EFC_{FBP17} and $EFC\Delta N_{CIP4}$, respectively, Figures 1B, 1C, 1E, and 1F). The dimer interfaces are mainly hydrophobic, with several charged residues, and involve several prominent patches of conserved residues (Figures S3A and S3B). One of the patches is located close to the rotational axis between two monomers and consists of the most highly conserved residues, Arg35, Glu39, Tyr42, Leu46, and the surrounding residues in helix α2 (Figures S1B, S3B, and S3C). The replacement of Tyr42 with Glu drastically reduced the solubility of a longer CIP4 fragment, EFC_{CIP4} (residues 1–303), in the cell-free translation (data not shown), indicating the importance of dimer formation in the function of the EFC domain. Another patch of conserved residues was identified in the more distal part of the dimer interface on helices α3 and α4 (Figure S3B). The conserved residues in this patch bind to the latter half of the EEP of the second molecule (Figures S3B and S3D). A CIP4 fragment lacking the EEP was expressed as a soluble protein in the cell-free translation (data not shown), suggesting that the EEP is not critical for dimer formation but stabilizes the formed dimer. The high conservation of the residues involved in the dimer interfaces suggests that all of the PCH proteins adopt similar dimeric structures.

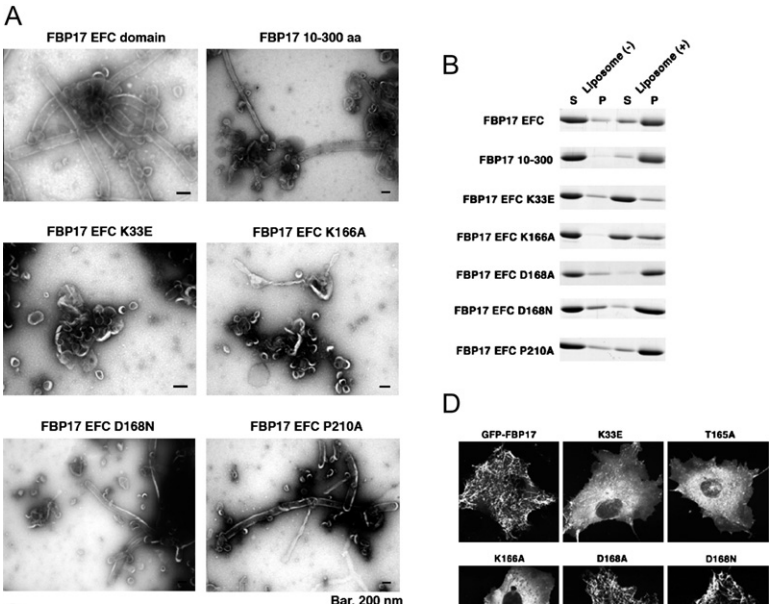

C

	liposome binding (%)	Liposome tubulation
FBP17 EFC	82%	++++
FBP17 10-300	91%	++
EFC K33E	18%	-/+
EFC T165A	N/A	N/A
EFC K166A	31%	-/+
EFC D168A	94%	N/A
EFC D168N	87%	+++
EFC D168R	N/A	N/A
EFC P210A	80%	+++

Figure 2. Membrane Binding and Tubulation Activities of the Wild-Type EFC_{FBP17} and Its Mutants

(A) Negative staining electron microscopy. Liposomes (0.2 mg/ml) were incubated with the indicated EFC-domain proteins (0.1 mg/ml) and were then observed by electron microscopy.

(B) Liposome-binding assay by sedimentation. The indicated proteins (0.1 mg/ml) were incubated with or without liposomes (1 mg/ml) made with brain lipids. After centrifugation, the pellet (P) and the supernatant (S) were analyzed by SDS-PAGE.

(C) Summary of the tubulation and the binding ability of the indicated proteins. Proteins cosedimented with liposomes (P) are expressed as percentages of the total protein (S + P). The relative tubulation ability of each protein is expressed as ++++ (very strong), +++ (strong), ++ (moderate), + (weak), or −/+ (almost nothing). N/A: not available.

(D) COS-7 cells were transfected with GFP-tagged, full-length FBP17 bearing each mutation, and the localization of FBP17 was observed by GFP fluorescence.

To confirm that the EFC domain exists as a dimer in solution, we measured the molar masses of the EFC-domain fragments by analytical ultracentrifugation (Figure S4). Sedimentation equilibrium analyses of EFC_{FBP17} and EFC_{CIP4} yielded molecular masses of 71.5 and 72.1 kDa, which are very close to the masses expected for the EFC_{FBP17} dimer (72.0 kDa) and EFC_{CIP4} dimer (71.4 kDa), respectively, based on their primary structures. No evidence was found for the presence of either monomeric or higher oligomeric species in the sedimentation velocity experiment (data not shown). Therefore, EFC_{FBP17} and EFC_{CIP4} exist almost exclusively as dimers under these measurement conditions.

The EFC Domain Binds to the Phospholipid Membrane with Its Concave Surface

The surface representation of the EFC domain revealed clustering of positively charged residues in wide areas of the concave surfaces (Figures 1G–1I and S2C–S2E). The conserved residues are also clustered, especially on the concave surface (Figures 1J–1L). Therefore, the positively charged, conserved residues on the concave surface may be important for the interaction of the EFC domain with the phospholipid membrane. In agreement with this prediction, several double mutations of the positively charged residues on the concave surface of EFC_{FBP17}, such as K33Q+R35Q, K51Q+K52Q, and R113Q+K114Q, reduced the membrane association and tubulation in vitro and impaired the in vivo membrane invagination induced by the overexpression of EFC_{FBP17} (Tsujita et al., 2006; Figure 1L). To confirm this hypothesis, we introduced point mutations into the residues on the concave surface of EFC_{FBP17}. The replacement of Lys33 with Glu significantly reduced the membrane binding and tubulation activities in vitro (Figures 1L and 2A–2C). This mutation also abolished the membrane invagination induced by GFP-FBP17 in vivo (Figure 2D). In contrast, the replacement of Asp168 with Ala did not significantly affect the membrane-binding and tubulation activities (Figures 1L and 2A–2C). In addition to this mutation, the D168N and D168R mutations also did not affect the membrane invagination induced by GFP-FBP17 in vivo (Figure 2D). These results indicate that the EFC domain binds and tubulates the phospholipid membrane by electrostatic interactions, using the positively charged residues distributed on its concave surface.

The EFC and BAR Domains Bind to and Induce Tubular Membranes with Different Diameters

The EFC domain forms an antiparallel, six-helix bundle in the middle of the dimer, which is a structural feature shared with the BAR domain and the IRSp53/MIM

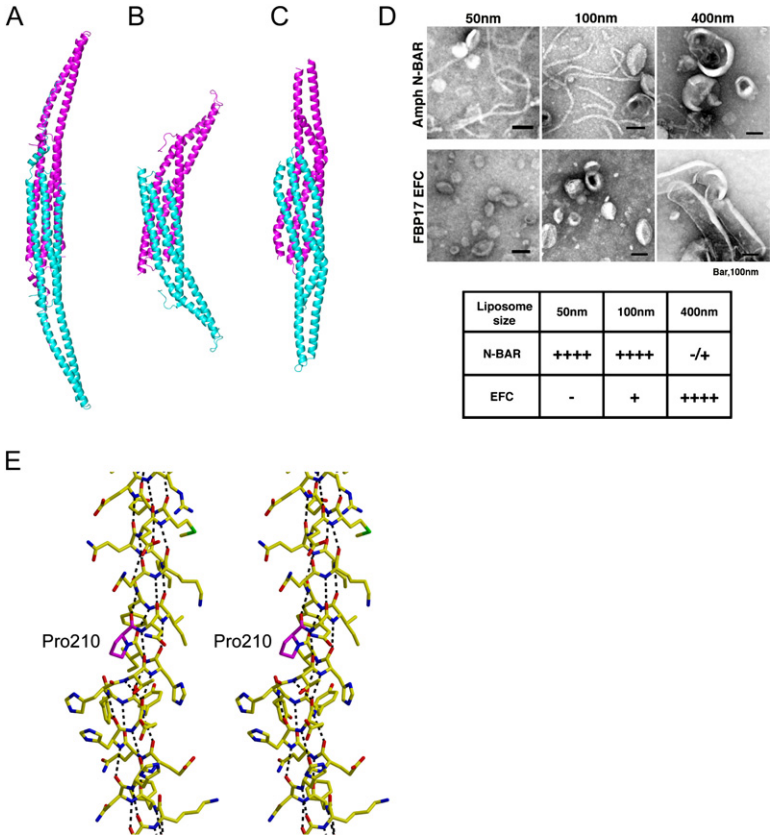

Liposome size	50nm	100nm	400nm
N-BAR	++++	++++	-/+
EFC	-	+	++++

Figure 3. Three-Dimensional Structures of the EFC Domain, Amphiphysin BAR Domain, and IRSp53 IMD

(A–C) Ribbon diagrams of the dimers of (A) EFC_{FBP17}, (B) amphiphysin BAR domain, and (C) IRSp53 IMD. The first and second molecules are colored cyan and magenta, respectively.

(D) Negative staining electron microscopy. Liposomes of defined maximum diameters (0.2 mg/ml), made with a filter apparatus, were incubated with N-BAR- or EFC-domain proteins (0.1 mg/ml) and then were observed by electron microscopy. The degree of tubulation is expressed in the table as ++++ (very strong), + (weak), or −/+ (almost nothing).

(E) A stereo figure of Pro210 and the surrounding residues in helix α4. Pro210 is colored magenta. Note that Pro210 breaks the hydrogen bonds in helix α4, thereby introducing a kink. Residues are shown as stick models.

homology domain (IMD) (Peter et al., 2004; Millard et al., 2005; Suetsugu et al., 2006; Masuda et al., 2006; Figures 3A–3C). The BAR domain is involved in membrane binding, membrane curvature sensing, and membrane tubulation (Takei et al., 1999; Peter et al., 2004). Positively charged residues on the concave surface of the BAR domain are important for its binding to and tubulation of the negatively charged phospholipid membrane (Peter et al., 2004), in a manner similar to that of the phospholipid-binding residues of the EFC domains.

Although the EFC and BAR domains share similar dimeric architectures, several aspects of the EFC-domain structure are markedly different from those of the BAR domain. First, helices α3 and α4 are more than 20 residues longer than the corresponding helices of the BAR domain, resulting in a more elongated molecular shape (Figures 3A and 3B). Second, the diameter of the tubular membrane that fits the concave surface of the EFC dimer (~600 Å) is larger than those of the *Drosophila* amphiphysin BAR domain (~220 Å) and the human endophilin BAR domain (~280 Å) (Peter et al., 2004; Masuda et al., 2006; Figures 3A and 3B). This larger diameter is partly due to the smaller intersection angle between the three long helices of the first and second molecules in the dimer (Figures 3A and 3B). Consistent with this, the dimer-interface residues are not conserved between the EFC and BAR domains. The present finding that the EFC and BAR domains fit different diameters of tubular membrane correlates well with the fact that the diameter of the EFC-induced tubular membrane is several times larger than that of the BAR-induced one (Itoh et al., 2005; Tsujita et al., 2006).

To address whether the BAR domain and the EFC domain exhibit different selectivity for the sizes of the liposomes, the tubulation activities of the amphiphysin N-BAR domain and EFC_{FBP17} were compared using liposomes with various defined diameters (Figure 3D). The N-BAR domain exhibited the highest tubulation activity for liposomes with diameters of 50 and 100 nm, while EFC_{FBP17} was more selective for liposomes with diameters larger than 100 nm (Figures 2A and 3D). Thus, the EFC domain is more selective for liposomes with lower curvature than the BAR domain, as expected from their structures. Note that the amphiphysin N-BAR domain can induce a longer tubular membrane than that expected from a single liposome, which suggests that it fuses liposomes upon tubulation, as reported for the endophilin N-BAR domain (Gallop et al., 2006). Parts of helices α3 and α4 form a long, kinked, coiled-coil structure protruding from the six-helix bundle (Figures 1B and 1C). A kink is caused in helix α4 by Pro210 (Figure 3E). This Pro residue is strictly conserved among the FCRP proteins (Figure S1B) but is replaced by other amino acids in the other subfamilies, such as *S. pombe* Cdc15, mammalian PACSINs/syndapins/FAP52, PSTPIP1, PSTPIP2/MAYP,

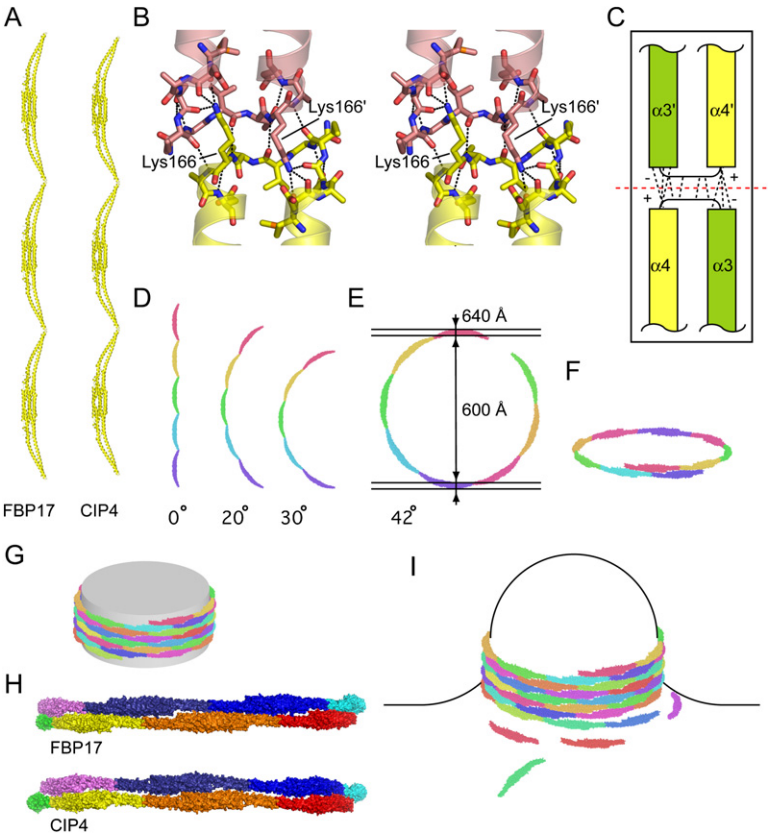

Figure 4. The EFC Filaments in the Crystals and a Model of Membrane Tubulation by the EFC Domain

(A) Filamentous structures of EFC_{FBP17} (left) and $EFC\Delta N_{CIP4}$ (right) in the crystals.

(B) A stereo figure of the dimer-dimer interfaces of the EFC_{FBP17} filament. Broken lines indicate hydrogen bonds. Lys166 is labeled. The prime symbol denotes residues in the symmetry-related molecule.

(C) A schematic representation showing the dimer-dimer interfaces. Helices α3 and α4 are indicated. The prime symbol denotes helices in the symmetry-related molecule. The "−" and "+" symbols indicate negative and positive charges at the carboxyl and amino termini of helices α3 and α4, respectively. The black broken lines indicate the hydrogen bonds in the interfaces. The red broken line indicates the hinge axis around which the dimer-dimer interfaces bend.

(D) The FBP17 EFC filaments, bent around the hinge region by 0, 20, or 30 degrees. Each EFC dimer is colored differently.

(E) A ring-like EFC filament, bent around the hinge by 42 degrees. The inner and outer diameters of the ring are indicated.

(F) A spiral filament.

(G) A spiral filament winding around a cylinder.

(H) Surface representations of the stacked EFC spirals of FBP17 (upper) and CIP4 (bottom), viewed from the convex side. Each EFC dimer is colored differently. The EFC filaments are placed to minimize the spaces between the two adjacent filaments. Note that the relative positions of the two adjacent filaments are different between FBP17 and CIP4.

(I) Schematic illustration showing how the EFC domain tubulates the lipid membrane from a liposome. An elongating EFC filament and the incoming EFC dimers are shown around a nascent tubular membrane.

and NOSTRIN (Figure S1B and data not shown). In order to determine if Pro210 is important for the gently curved overall shape of the dimer (Figures 1B and 3A), a mutant of EFC_{FBP17} with Pro210 replaced by Ala was prepared and tested for its membrane-binding and tubulation activities. The P210A mutation did not affect the activities (Figures 2A–2D) but modestly increased the diameter of the induced tubular membrane (Figure S5). Therefore, the Pro210-induced kink in helix α4 participates in the mechanism that forms the gently curved shape and is likely to play a role in fine tuning of the curvature.

Filament Formation by the EFC-Domain Dimer

Besides the interface for dimerization, we found additional common crystal-packing interfaces between the crystals of the two EFC domains; the dimers are arranged to form filaments (Figure 4A). These interfaces involve several hydrogen-bonding interactions between the neighboring symmetry-related dimers (Figures 4B, 4C, S6A, and S6B). First, the main-chain carbonyl and imino groups in the loop for the turn from helix α3 to helix α4 (Figure 4C) form four hydrogen bonds (Figures 4B, S6A, and S6B) in the dimer-dimer interface. Second, Lys166, which is conserved in the FCRP proteins (Figure S1B), forms hydrogen bonds with three main-chain carbonyl groups of the adjacent dimer (Figures 4B and S6A). Furthermore, Thr165 is conserved in the α3–α4 loop (Figures 1L, S1B, and S6B). Thr165 is not directly involved in the dimer-dimer interactions in the filament in the crystals (Figures 1L and S6B). However, it contributes to the turn conformation by hydrogen bonding with the main-chain imino group of Asp168. These intensive interactions seem to stabilize the filamentous structure of the EFC-domain dimers in the crystals (Figure 4A). Interestingly, filament formation by the FBP17 EFC domain was observed by electron microscopy in the absence of liposomes (Itoh et al., 2005). The length of the EFC dimer in the filament in the crystals corresponds well to that of one unit of the periodic structure in the EFC filament, observed by negative staining EM (Itoh et al., 2005). The $EFC\Delta N_{CIP4}$ crystals grew in the purification buffer without any precipitant, indicating that the filament in the crystals is similar to that formed under some solution conditions.

The replacement of Lys166 with Ala reduced both the membrane-binding and tubulation activities of EFC_{FBP17} (Figures 1L, 2A–2C, and 4B). Moreover, the T165A and K166A mutations both abolished the induction of membrane invagination by FBP17 in cells (Figures 1L and 2D). These

results demonstrate the importance of filament formation in membrane binding and tubulation by the EFC domain.

The EFC filament adopts a straight, periodic conformation in the crystals, and the observed dimer-dimer interfaces of the EFC filament seem to be flexible and to form a hinge in the filament (Figures 4A–4C). When the EFC filament bends at the hinges, the overall shape of the filament becomes round (Figures 4D, S6C, and S6D). Finally, a ring or spiral is formed (Figures 4E and 4F), which may wind around the nascent tubular membrane to support the tubular shape, with the concave dimer surfaces facing the tubular membrane (Figure 4G). When the EFC spiral winds around the tubular membrane several times, lateral interactions between the neighboring filaments may be formed. The shapes of the EFC filaments are quite complementary, and the tight spiral can cover the tubular membrane with minimal uncovered areas and with no severe clashes (Figure 4H). Helix α1 is one of the structural elements that directly support the lateral interface residues (Figure 4H). Interestingly, EFCΔN_{FBP17}, which lacks the N-terminal nine residues including helix α1, showed a reduced tubulation activity, while its membrane-binding activity was not affected (Figures 2A–2C). Since the EFC domain is assumed to bind most tightly to the properly curved membrane, the EFC dimers may accumulate at the foot of the nascent tubular membrane and join the preformed EFC filament to drive continuous membrane tubulation (Figure 4I).

Tubular Membrane Striation with the EFC Filaments

Phase-contrast cryo-TEM with a Zernike phase plate allows the observation of biological specimens with high contrast (Danev and Nagayama, 2001), without any staining (Nagayama, 2005). Among the tubular membranes observed by the phase-contrast cryo-TEM, we certainly found those with striated structures, which probably represent the tight EFC spirals covering the tubular membranes (Figures 5A–5C). The striations seemed to be nearly perpendicular to the main axis of the tubular membrane, and the average spacing between neighboring striations in Figure 5C was ~41 Å, where the regularly spaced striations gave rise to diffraction peaks in the Fourier image, as shown in Figure 5D. The spacing of the striations ranges from 40 Å to 50 Å (Figures 5A–5C), and the minimum striation pitch agrees fairly well with the width of the thickest part of the EFC filament in the crystals (~35 Å). These properties correspond quite well to our model of membrane tubulation (Figure 4I).

The diameters of the EFC-induced tubular membranes observed by the negative staining EM range from 600 to 2000 Å or 400 to 2000 Å (Figure S5 and Itoh et al., 2005). On the other hand, those observed by the phase-contrast cryo-TEM range from 650 Å to 3300 Å. The maximum diameter of the tubular membrane may be larger because the EFC filaments were also observed on round liposomes with larger diameters (>1 μm; data not shown). These observations suggest that the EFC domain binds to liposomes with various diameters and constrains them into tubules with diameters of 650 Å or larger (Figures 5A–5C). Note that the minimum diameter of the observed tubular membranes is close to that of the tubular membrane that fits the concave surface of the EFC domain (~600 Å). We also observed a snapshot of a possible intermediate state of membrane tubulation in which the EFC-coated tubular membrane protrudes from a parental liposome (Figure 5A).

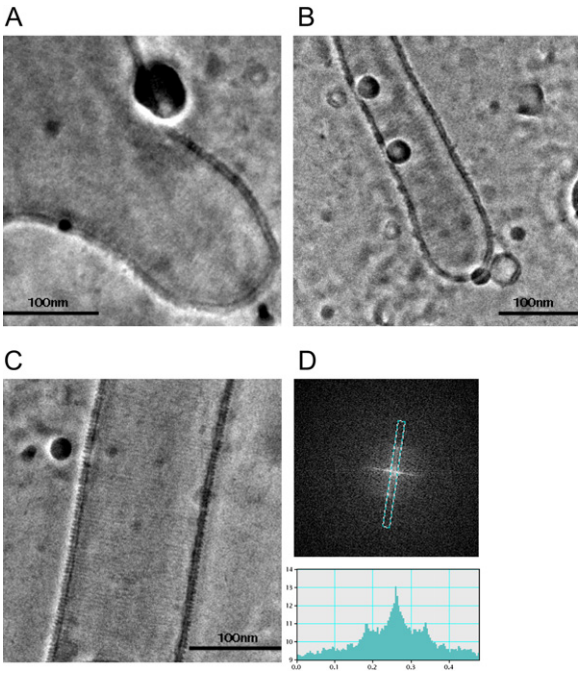

Figure 5. Striated Tubular Membranes Coated with the EFC Ring/Spirals, Observed by Phase-Contrast Cryo-TEM in Vitrified Ices

(A) A nascent tubular membrane protruding from a parental liposome. The spacing of the striations ranges from 40 Å to 50 Å (average spacing ~44 Å).

(B) A narrow tubular membrane covered with sparse EFC spirals (average spacing ~42 Å).

(C) A tubular membrane showing clear and regular striations (average spacing ~41 Å).

(D) A Fourier image of the striations shown in Figure 5C (upper). A cross-section of diffraction in the Fourier image, showing a regular spacing of about 40 Å (lower).

FBP17 Is Recruited to CCPs in the Late Stage of CME

Knockdown experiments implicated FBP17 in the receptor-mediated endocytosis of cholera toxin subunit B (CTB), epidermal growth factor (EGF), and transferrin (Kamioka et al., 2004; Itoh et al., 2005; Tsujita et al., 2006). Consistent with this, CTB, EGF, and transferrin colocalized with the FBP17-induced tubular membranes (Kamioka et al., 2004; Tsujita et al., 2006). Thus, FBP17 is involved in both clathrin-dependent and -independent endocytosis. CIP4 and Toca-1 are also implicated in CME (Itoh et al., 2005; Tsujita et al., 2006). To further

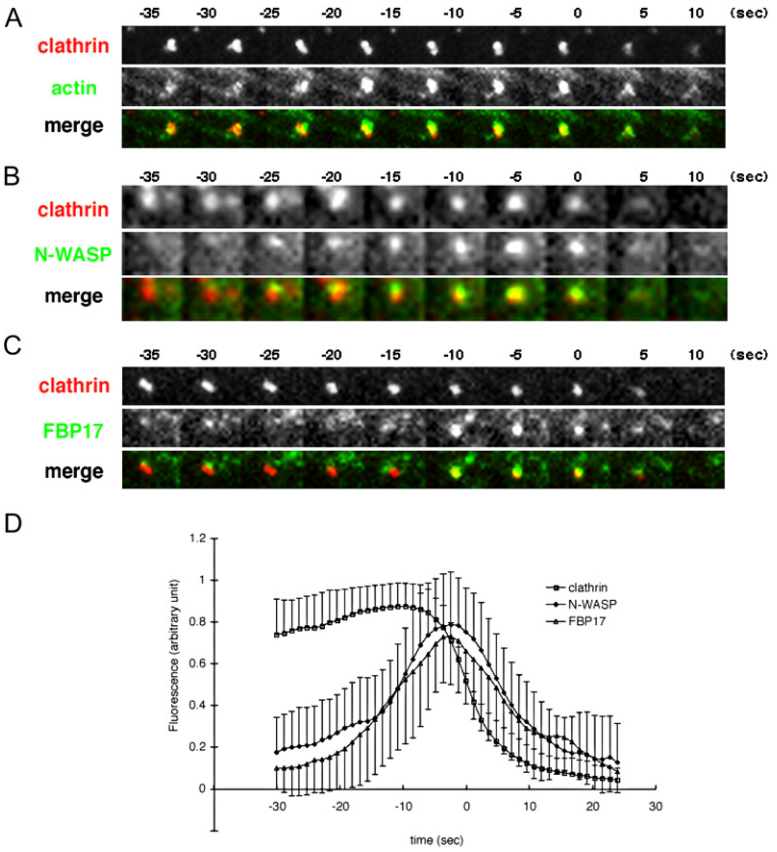

Figure 6. Actin, N-WASP, and FBP17 Are Recruited to CCPs in the Late Step of CME

DsRed-monomer-tagged clathrin light chain and GFP-tagged actin (A), N-WASP (B), or FBP17 (C) were observed by total-internal-reflection microscopy. The time of 50% decrease of the DsRed-clathrin fluorescence was set to 0. The normalized fluorescence intensities of clathrin, N-WASP, and FBP17 were plotted over time, and the averages of 30–40 events are shown in (D). Bars indicate standard deviation.

address the role of FBP17 in CME, we used total internal reflection fluorescence microscopy (TIRFM) to test whether and when FBP17 is recruited to CCPs. Actin and N-WASP were reportedly transiently recruited to CCPs in the late stage of CME (Perrais and Merrifield, 2005; Merrifield et al., 2004; Yarar et al., 2005; Figures 6A and 6B). FBP17 was also recruited to CCPs for a time period very similar to that of N-WASP, when clathrin departed from the plasma membrane (Figures 6B–6D).

DISCUSSION

We have shown that FBP17 was transiently recruited to CCPs in the late stage of CME, and that its retention time roughly corresponds to those of actin and N-WASP (Figures 6A–6D). Based on these and other data, we propose the following hypothetical model for the role of FBP17 and other FCRP proteins in CME. Clathrin coats that can accommodate a transport vesicle form a variety of structures with various diameters larger than ~700 Å (Fotin et al., 2004). Interestingly, the EFC domain is selective for liposomes larger than 1000 Å in diameter, and it generates tubular membranes with diameters larger than 650 Å. Hence, it is possible that the EFC domain of the FCRP proteins senses the lower curvature at the foot of hemispherical CCPs and accumulates at the beginning of the invagination step (Figure 7). Subsequent self-oligomerization of the EFC domain may drive CCP invagination (Figure 7). Finally, the FCRP proteins may recruit dynamins with the SH3 domain, to further narrow the diameter of the invaginated tube to ~200 Å (nonconstricted state) and to ~100 Å (constricted state) for scission to take place (Figure 7; Chen et al., 2004). The FCRP proteins may also activate the actin nucleation machinery, such as N-WASP, at the foot of the CCP, and this machinery may cooperate with dynamins to regulate endocytic vesicle scission (Merrifield et al., 2005; Itoh et al., 2005; Tsujita et al., 2006). Thus, the FCRP proteins may link clathrin-mediated budding to dynamin-dependent scission through their interaction with the membrane by the EFC domain in CME.

We observed that FBP17 was colocalized with CCPs (Figure 6). This result supports our model in which the FCRP proteins are recruited to CCPs in the invagination step after the clathrin assembly. Since the BAR domain binds and deforms smaller liposomes than those preferred by the EFC domain (Figure 3), the BAR-domain proteins may be recruited to CCPs for a shorter time period after the recruitment of the EFC-domain proteins, i.e., just before or during the scission step. Thus, although they share similar dimeric architectures, the PCH proteins and the BAR-domain proteins may function at distinct steps in endocytic vesicle formation due to the differences in their overall structures.

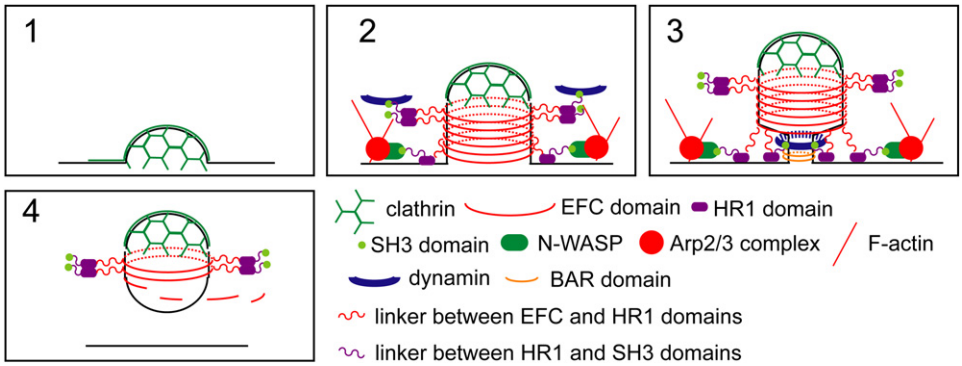

Figure 7. A Model for Coordinated Clathrin Assembly, Invagination, and Scission at a Single CCP

(1) First, the clathrin coats assemble. (2) Second, the EFC domain of the FCRP proteins senses the curvature of the clathrin-coated bud and polymerizes to drive CCP invagination. Concomitant actin polymerization may take place at the foot of the CCP. The SH3 domain recruits N-WASP and the Arp2/3 complex for actin polymerization. Simultaneously, the SH3 domain also recruits dynamins. (3) The BAR-domain proteins are recruited to the narrowed tubular membrane induced by the FCRP, N-WASP-induced actin polymerization, and the mechanical activity of dynamin. The BAR-domain proteins then continue to recruit dynamin and/or N-WASP to the narrowed tubules. (4) Finally, a CCV leaves from the plasma membrane.

EXPERIMENTAL PROCEDURES

Initial Expression Trials

Twenty-six DNA constructs, encoding human CIP4 fragments with different N- and C-terminal boundaries, were amplified from the human full-length cDNA clone, with the NCBI protein database code gi:62897779. The amplified cDNA fragment was attached by overlap PCR to the T7 promoter sequence, the ribosome-binding site, the His-tag, the cleavage site for tobacco etch virus (TEV) protease, and the T7 terminator sequence (Horton et al., 1989).

The fusion proteins were synthesized by the dialysis mode of the cell-free protein expression system using PCR DNA templates, as described (Kigawa et al., 1999, 2004; Sitaraman et al., 2004). The total reaction mixtures were centrifuged to remove the insoluble proteins, and the total and soluble fractions were subjected to SDS-PAGE to assess the quantity and the solubility of the expressed proteins.

Protein Preparations

The selenomethionine (SeMet)-substituted EFCΔN_{CIP4} was synthesized in the cell-free system as a His-tagged protein with a TEV protease site. The protein was purified on a HisTrap column (Amersham Biosciences), eluted with imidazole, cleaved with TEV protease, and further purified by anion-exchange and gel-filtration chromatography. The protein ran as a single band on an SDS-PAGE gel and was concentrated to approximately 3.8 mg/ml, using an Amicon Ultra-15 centrifugal concentrator (Millipore), prior to crystallization.

The SeMet-substituted human EFC_{FBP17} was expressed as a GST-fusion protein in *E. coli* B834 (DE3) (Novagen). The GST-fusion protein was purified with Glutathione Sepharose HP, eluted by reduced glutathione, cleaved by PreScission protease, and further purified by anion-exchange and gel-filtration chromatography. The protein ran as a single band on an SDS-PAGE gel and was concentrated to approximately 0.8–1.0 mg/ml in the same manner as for EFCΔN_{CIP4}. EFC_{FBP17} mutants were prepared in a similar manner to that for EFC_{FBP17}. Point mutations were introduced by the QuickChange protocol (Stratagene). More detailed procedures are described in the Supplemental Data.

Crystallization, Data Collection, and Structure Determination

The EFCΔN_{CIP4} crystals were grown at 4°C in 20 mM Tris-HCl buffer (pH 8.0) containing 150 mM NaCl and 2 mM DTT. The crystals belong to the space group C2, with unit-cell dimensions of a = 94.8 Å, b = 70.4 Å, c = 65.7 Å, and β = 107.2°. The crystals were transferred to a solution containing 200 mM tri-sodium citrate dihydrate, 20% polyethylene glycol (PEG) 3350, and 10% glycerol and were flash-cooled in liquid nitrogen. A MAD data set was collected at the Southeast Regional Collaborative Access Team (SER-CAT) 22-ID beamline at the Advanced Photon Source, Argonne National Laboratory (Table 1). A high-resolution data set was collected at the RIKEN Structural Genomics Beamline I (BL26B1) at SPring-8 (Table 1). Data were processed with the HKL2000 program package (Otwinowski and Minor, 1997). Initial phases were obtained with the MAD data set, and a readily interpretable electron density map was calculated after density modification using the program CNS (Brunger et al., 1998). The initial model was built with the program O (Jones et al., 1991). The model was refined with the program CNS against the high-resolution data set. Iterative rounds of refinement and model rebuilding improved the quality of the simulated-annealing omit electron density maps, allowing us to build additional residues in the model. The final model has an R_{work} of 22.8% and an R_{free} of 27.9% at 2.3 Å resolution.

The EFC_{FBP17} crystals were grown at 20°C, using the hanging-drop vapor-diffusion method, against 50 mM MES-NaOH buffer (pH 6.0) containing 20 mM $MgCl_2$ and 15% isopropanol. The crystals belong to the space group C2, with unit-cell dimensions of a = 201.0 Å, b = 41.4 Å, c = 56.5 Å, and β = 105.1°. The crystals were transferred to a reservoir solution containing 25% glycerol as a cryoprotectant and were flash-cooled in liquid nitrogen. A native data set was collected at BL26B1 at SPring-8 (Table 1). The data were processed with the HKL2000 program package. The structure of EFC_{FBP17} was determined by the molecular replacement method, using the structure of EFCΔN_{CIP4} as a search model, with the program CNS. The model building was completed in a similar manner to that for EFCΔN_{CIP4} with the programs CNS and O. The final model has an R_{work} of 21.2% and an R_{free} of 26.7% at 2.6 Å resolution.

Figures were created using the programs MolScript (Kraulis, 1991), Raster3D (Merritt and Murphy, 1994), PyMol (http://www.pymol.org), and O. The buried surface areas were calculated by the program AREAIMOL of the CCP4 suit of programs (CCP4, 1994).

Liposome Preparation and Binding Assay

The liposome-binding assay was performed as described (Peter et al., 2004). Liposomes were made from total bovine brain lipids (Folch fraction 1, Sigma). Dried lipids were resuspended in 20 mM Hepes (pH 7.4), 150 mM NaCl, and 1 mM DTT by mixing with a vortex followed by hydration at 37°C for 1 hr. This preparation resulted in the formation of a mixture containing large-diameter (~1 μm) liposomes. Proteins (10 μg) were incubated with liposomes (100 μg) in 100 μl of buffer for 15

Table 1. Data Collection, Phasing, and Refinement Statistics

		$EFC\Delta N_{CIP4}$		EFC_{FBP17}
		Peak	Edge	
Diffraction Data				
Temperature (K)	100	100	100	100
Space group	*C*2	*C*2	*C*2	*C*2
Wavelength (Å)	1.0000	0.9794	0.9795	1.0000
Resolution (Å)	50.0–2.3	50.0–2.5	50.0–2.5	50.0–2.6
Unique reflections	16924	13557	13274	12632
Total reflections	82936	99326	94288	75084
$I/\sigma(I)$	21.0 (3.5)	23.0 (8.8)	29.0 (8.2)	17.1 (4.6)
R_{merge} [a] (%)	7.2 (31.7)	6.8 (14.2)	6.1 (14.4)	10.1 (26.0)
Completeness (%)	91.7 (61.2)	94.0 (71.7)	91.3 (62.1)	90.8 (62.3)
Phasing Statistics				
Number of sites		7	7	
R_{cullis} (anomalous) acentrics		0.6049	0.7130	
Mean over all figure of merit acentrics			0.5464	
Refinement Statistics				
Protein atoms	2238			2347
Water oxygens	139			120
R_{work} [b] (%)	22.8			21.2
R_{free} [c] (%)	27.9			26.7
Rms deviation from ideal values				
Bond length, Å	0.006			0.007
Bond angles, degrees	1.0			1.0
Average B factor, $Å^2$				
Protein	59.8			46.3
Solvent	63.6			54.5

Values in parentheses are for the highest resolution shell.
[a] $R_{merge} = \sum_h \sum_i |I_{h,i} - \langle I_h \rangle| / \sum_h \sum_i |I_{h,i}|$, where $_h$ refers to unique reflection indices and *i* indicates symmetry-equivalent indices.
[b] $R_{work} = \sum |F_O - F_C| / \sum |F_O|$ for the working set reflections (90% of the data) used for the refinement.
[c] $R_{free} = \sum |F_O - F_C| / \sum |F_O|$ for the test set reflections (10% of the data) excluded from the refinement.

min at room temperature and were centrifuged at 60,000 rpm for 15 min at 25°C in a TL 100 rotor (Beckman). Supernatants and pellets were subjected to SDS-PAGE, and the gels were stained with Coomassie Brilliant Blue. Liposomes with a defined maximum diameter (50, 100, and 400 nm) were made by extrusion of the liposomes, prepared as described above, through polycarbonate filter membranes (Avanti Polar Lipids).

Negative Staining Electron Microscopy

Purified proteins (0.1 mg/ml) were incubated with liposomes (0.2 mg/ml), prepared as above, in 20 mM Hepes buffer (pH 7.5) containing 150 mM KCl, 1 mM EDTA, and 1 mM DTT at 25°C for 20 min. This mixture was applied to glow-discharged collodion- and carbon-coated copper grids, which were washed in 100 mM Hepes (pH 7.9). The grids were stained with 2% uranyl acetate. At each step, excess solution was removed by filter paper. Dried grids were examined using an electron microscope (JEOL).

Phase-Contrast Cryo-TEM

Purified proteins (0.5 mg/ml) were incubated with liposomes (0.5 mg/ml) in 20 mM Hepes buffer (pH 7.5) containing 100 mM KCl and 1 mM EDTA at 37°C for 15 min. Samples were dropped on a copper grid coated with holey carbon film (Quantifoil). After blotting the excess liquid carefully with the tip of a filter paper, to make a thin vitreous film, the sample was frozen rapidly in liquid ethane using a LEICA rapid-freezing apparatus (LEICA EM CPC). The vitrified specimen was transferred to the pre-cooled specimen chamber of the TEM using a cryo-transfer system. The experiments were carried out on a JEOL JEM-3100FFC electron microscope equipped with a helium stage and operated at 300 kV acceleration voltage with the minimum dose system and Zernike phase plates (Danev and Nagayama, 2001).

Cell Culture and Microscopy

GFP-FBP17 was prepared as described previously (Tsujita et al., 2006). GFP-actin was purchased (Clontech). To obtain GFP-N-

WASP, N-WASP was subcloned into the pEGFP vector (Suetsugu et al., 2002). The human clathrin light chain cDNA was obtained by PCR of human brain cDNA and was subcloned into the pDsRed-monomer-C1 vector (BD Biosciences). COS-7 cells and NIH 3T3 cells were maintained in DMEM containing 10% FCS and CS, respectively. Transfection was performed using Lipofectamine 2000 (Invitrogen), according to the manufacturer's protocol. Fluorescent images were taken through a microscope (Nikon) with a confocal microscopy system (Biorad; Radiance 2000) at RT. The 60× oil immersion objective NA = 1.40 (Nikon) was used. For live observation with total internal reflection microscopy, NIH 3T3 cells were grown on a glass-bottomed dish. The images were acquired for 5–10 min at 5 s intervals with a total-internal-reflection (TIRF) microscopy system (Olympus) with a 100× oil immersion objective NA = 1.45 (Olympus) and the MetaMorph software. All images were processed with imageJ (NIH) and Photoshop (Adobe). For each spot of clathrin in the TIRF images, the fluorescence intensity was plotted over time. The fluorescence intensity was normalized for each event of clathrin disappearance (endocytosis) from the TIRF images. The average and the standard deviations were calculated.

Supplemental Data

Supplemental Data include Experimental Procedures and six figures and can be found with this article online at http://www.cell.com/cgi/content/full/129/4/761/DC1/.

ACKNOWLEDGMENTS

We thank S. Morita, Y. Kinoshita, K. Nagano, H. Tochio-Uda, N. Maoka, Y. Tomabechi, H. Hamana, N. Obayashi, S. Tojo, M. Ueno, S. Oojimi, K. Honda, K. Usui, M. Aoki, M. Inoue, K. Katsura, and T. Tanaka for sample preparations and Drs. R. Danev and H. Shigematsu for help in the cryo-TEM data collection and for fruitful discussions. We thank Dr. T. Itoh (Institute of Medical Science, The University of Tokyo) for technical support and helpful discussions. We also thank Dr. K. Toyooka and his colleagues at the RIKEN Plant Science Center for electron microscopy. X-ray data were collected at the RIKEN Structural Genomics Beamline I (BL26B1) at SPring-8 and at the Southeast Regional Collaborative Access Team (SER-CAT) 22-ID beamline at the Advanced Photon Source, Argonne National Laboratory. Supporting institutions may be found at http://www.ser.anl.gov/new/members.html. Use of the Advanced Photon Source was supported by the US Department of Energy, Office of Science, Office of Basic Energy Sciences under Contract No. W-31-109-Eng-38. This work was supported by the RIKEN Structural Genomics/Proteomics Initiative (RSGI), the National Project on Protein Structural and Functional Analyses, Ministry of Education, Culture, Sports, Science and Technology of Japan. This work was also supported by grants-in-aid for Scientific Research on Priority Areas from the Ministry of Education, Culture, Sports, and Technology of Japan and from the Japan Science and Technology Corporation (JST).

Received: July 10, 2006
Revised: January 18, 2007
Accepted: March 2, 2007
Published: May 17, 2007

REFERENCES

Aspenström, P. (1997). A Cdc42 target protein with homology to the non-kinase domain of FER has a potential role in regulating the actin cytoskeleton. Curr. Biol. *7*, 479–487.

Brunger, A.T., Adams, P.D., Clore, G.M., DeLano, W.L., Gros, P., Grosse-Kunstleve, R.W., Jiang, J.S., Kuszewski, J., Nilges, M., Pannu, N.S., et al. (1998). Crystallography & NMR system: a new software suite for macromolecular structure determination. Acta Crystallogr. D Biol. Crystallogr. *54*, 905–921.

CCP4 (Collaborative Computational Project, Number 4) (1994). Acta Crystallogr. D Biol. Crystallogr. *50*, 760–763.

Chen, Y.J., Zhang, P., Egelman, E.H., and Hinshaw, J.E. (2004). The stalk region of dynamin drives the constriction of dynamin tubes. Nat. Struct. Mol. Biol. *11*, 574–575.

Danev, R., and Nagayama, K. (2001). Transmission electron microscopy with Zernike phase plate. Ultramicroscopy *88*, 243–252.

Dawson, J.C., Legg, J.A., and Machesky, L.M. (2006). Bar domain proteins: a role in tubulation, scission and actin assembly in clathrin-mediated endocytosis. Trends Cell Biol. *16*, 493–498.

Farsad, K., and De Camilli, P. (2003). Mechanisms of membrane deformation. Curr. Opin. Cell Biol. *15*, 372–381.

Ford, M.G., Mills, I.G., Peter, B.J., Vallis, Y., Praefcke, G.J., Evans, P.R., and McMahon, H.T. (2002). Curvature of clathrin-coated pits driven by epsin. Nature *419*, 361–366.

Fotin, A., Cheng, Y., Sliz, P., Grigorieff, N., Harrison, S.C., Kirchhausen, T., and Walz, T. (2004). Molecular model for a complete clathrin lattice from electron cryomicroscopy. Nature *432*, 573–579.

Gallop, J.L., Jao, C.C., Kent, H.M., Butler, P.J., Evans, P.R., Langen, R., and McMahon, H.T. (2006). Mechanism of endophilin N-BAR domain-mediated membrane curvature. EMBO J. *25*, 2898–2910.

Hinshaw, J.E., and Schmid, S.L. (1995). Dynamin self-assembles into rings suggesting a mechanism for coated vesicle budding. Nature *374*, 190–192.

Ho, H.Y., Rohatgi, R., Lebensohn, A.M., Ma, L., Li, J., Gygi, S.P., and Kirschner, M.W. (2004). Toca-1 mediates Cdc42-dependent actin nucleation by activating the N-WASP-WIP complex. Cell *118*, 203–216.

Horton, R.M., Hunt, H.D., Ho, S.N., Pullen, J.K., and Pease, L.R. (1989). Engineering hybrid genes without the use of restriction enzymes: gene splicing by overlap extension. Gene *77*, 61–68.

Itoh, T., and De Camilli, P. (2006). BAR, F-BAR (EFC) and ENTH/ANTH domains in the regulation of membrane-cytosol interfaces and membrane curvature. Biochim. Biophys. Acta *1761*, 897–912.

Itoh, T., Erdmann, K.S., Roux, A., Habermann, B., Werner, H., and De Camilli, P. (2005). Dynamin and the actin cytoskeleton cooperatively regulate plasma membrane invagination by BAR and F-BAR proteins. Dev. Cell *9*, 791–804.

Jones, T.A., Zou, J.Y., Cowan, S.W., and Kjeldgaard, M. (1991). Improved methods for building protein models in electron-density maps and the location of errors in these models. Acta Crystallogr. A *47*, 110–119.

Kaksonen, M., Toret, C.P., and Drubin, D.G. (2005). A modular design for the clathrin- and actin-mediated endocytosis machinery. Cell *123*, 305–320.

Kaksonen, M., Toret, C.P., and Drubin, D.G. (2006). Harnessing actin dynamics for clathrin-mediated endocytosis. Nature Rev. Mol. Cell Biol. *7*, 404–414.

Kamioka, Y., Fukuhara, S., Sawa, H., Nagashima, K., Masuda, M., Matsuda, M., and Mochizuki, N. (2004). A novel dynamin-associating molecule, formin-binding protein *17*, induces tubular membrane invaginations and participates in endocytosis. J. Biol. Chem. *279*, 40091–40099.

Kessels, M.M., and Qualmann, B. (2004). The syndapin protein family: linking membrane trafficking with the cytoskeleton. J. Cell Sci. *117*, 3077–3086.

Kigawa, T., Yabuki, T., Yoshida, Y., Tsutsui, M., Ito, Y., Shibata, T., and Yokoyama, S. (1999). Cell-free production and stable-isotope labeling of milligram quantities of proteins. FEBS Lett. *442*, 15–19.

Kigawa, T., Yabuki, T., Matsuda, N., Matsuda, T., Nakajima, R., Tanaka, A., and Yokoyama, S. (2004). Preparation of *Escherichia coli*

cell extract for highly productive cell-free protein expression. J. Struct. Funct. Genomics *5*, 63–68.

Kraulis, P.J. (1991). MolScript-a program to produce both detailed and schematic plots of protein structures. J. Appl. Crystallogr. *24*, 946–950.

Lippincott, J., and Li, R. (2000). Involvement of PCH family proteins in cytokinesis and actin distribution. Microsc. Res. Tech. *49*, 168–172.

Masuda, M., Takeda, S., Sone, M., Ohki, T., Mori, H., Kamioka, Y., and Mochizuki, N. (2006). Endophilin BAR domain drives membrane curvature by two newly identified structure-based mechanisms. EMBO J. *25*, 2889–2897.

McMahon, H.T., and Gallop, J.L. (2005). Membrane curvature and mechanism of dynamic cell membrane remodelling. Nature *438*, 590–596.

Merrifield, C.J., Qualmann, B., Kessels, M.M., and Almers, W. (2004). Neural Wiskott Aldrich Syndrome Protein (N-WASP) and the Arp2/3 complex are recruited to sites of clathrin-mediated endocytosis in cultured fibroblasts. Eur. J. Cell Biol. *83*, 13–18.

Merrifield, C.J., Perrais, D., and Zenisek, D. (2005). Coupling between clathrin-coated-pit invagination, cortactin recruitment, and membrane scission observed in live cells. Cell *121*, 593–606.

Merritt, E.A., and Murphy, M.E.P. (1994). Raster3D version 2.0. A program for photorealistic molecular graphics. Acta Crystallogr. D *50*, 869–873.

Miki, H., and Takenawa, T. (2003). Regulation of actin dynamics by WASP family proteins. J. Biochem. (Tokyo) *134*, 309–313.

Millard, T.H., Bompard, G., Heung, M.Y., Dafforn, T.R., Scott, D.J., Machesky, L.M., and Futterer, K. (2005). Structural basis of filopodia formation induced by the IRSp53/MIM homology domain of human IRSp53. EMBO J. *24*, 240–250.

Nagayama, K. (2005). Phase contrast enhancement with phase plates in electron microscopy. Ad. Imaging Elec. Phys. *138*, 69–146.

Otwinowski, Z., and Minor, W. (1997). Processing of X-ray diffraction data collected in oscillation mode. Methods Enzymol. *276*, 307–326.

Perrais, D., and Merrifield, C.J. (2005). Dynamics of endocytic vesicle creation. Dev. Cell *9*, 581–592.

Peter, B.J., Kent, H.M., Mills, I.G., Vallis, Y., Butler, P.J., Evans, P.R., and McMahon, H.T. (2004). BAR domains as sensors of membrane curvature: the amphiphysin BAR structure. Science *303*, 495–499.

Praefcke, G.J., and McMahon, H.T. (2004). The dynamin superfamily: universal membrane tubulation and fission molecules? Nat. Rev. Mol. Cell Biol. *5*, 133–147.

Pupko, T., Bell, R.E., Mayrose, I., Glaser, F., and Ben-Tal, N. (2002). Rate4Site: an algorithmic tool for the identification of functional regions in proteins by surface mapping of evolutionary determinants within their homologues. Bioinformatics *18* (*Suppl 1*), S71–S77.

Ren, G., Vajjhala, P., Lee, J.S., Winsor, B., and Munn, A.L. (2006). The BAR domain proteins: molding membranes in fission, fusion, and phagy. Microbiol. Mol. Biol. Rev. *70*, 37–120.

Roux, A., Uyhazi, K., Frost, A., and De Camilli, P. (2006). GTP-dependent twisting of dynamin implicates constriction and tension in membrane fission. Nature *441*, 528–531.

Schweitzer, S.M., and Hinshaw, J.E. (1998). Dynamin undergoes a GTP-dependent conformational change causing vesiculation. Cell *93*, 1021–1029.

Sitaraman, K., Esposito, D., Klarmann, G., Le Grice, S.F., Hartley, J.L., and Chatterjee, D.K. (2004). A novel cell-free protein synthesis system. J. Biotechnol. *110*, 257–263.

Suetsugu, S., Hattori, M., Miki, H., Tezuka, T., Yamamoto, T., Mikoshiba, K., and Takenawa, T. (2002). Sustained activation of N-WASP through phosphorylation is essential for neurite extension. Dev. Cell *3*, 645–658.

Suetsugu, S., Murayama, K., Sakamoto, A., Hanawa-Suetsugu, K., Seto, A., Oikawa, T., Mishima, C., Shirouzu, M., Takenawa, T., and Yokoyama, S. (2006). The RAC-binding domain/IRSP53-MIM homology domain of IRSP53 induces RAC-dependent membrane deformation. J. Biol. Chem. *281*, 35347–35358.

Takei, K., McPherson, P.S., Schmid, S.L., and De Camilli, P. (1995). Tubular membrane invaginations coated by dynamin rings are induced by GTP-γS in nerve terminals. Nature *374*, 186–190.

Takei, K., Slepnev, V.I., Haucke, V., and De Camilli, P. (1999). Functional partnership between amphiphysin and dynamin in clathrin-mediated endocytosis. Nat. Cell Biol. *1*, 33–39.

Takenawa, T., and Suetsugu, S. (2007). The WASP-WAVE protein network: connecting the membrane to the cytoskeleton. Nat. Rev. Mol. Cell Biol. *8*, 37–48.

Tsujita, K., Suetsugu, S., Sasaki, N., Furutani, M., Oikawa, T., and Takenawa, T. (2006). Coordination between actin cytoskeleton and membrane deformation by a novel membrane tubulation domain of PCH proteins is involved in endocytosis. J. Cell Biol. *172*, 269–279.

Yarar, D., Waterman-Storer, C.M., and Schmid, S.L. (2005). A dynamic actin cytoskeleton functions at multiple stages of clathrin-mediated endocytosis. Mol. Biol. Cell *16*, 964–975.

Zimmerberg, J., and Kozlov, M.M. (2006). How proteins produce cellular membrane curvature. Nat. Rev. Mol. Cell Biol. *7*, 9–19.

Accession Numbers

The coordinates and structure factors have been deposited in the Protein Data Bank with the ID codes 2EFK and 2EFL for the EFCΔN_{CIP4} and EFC_{FBP17} structures, respectively.